JACS
JOURNAL OF THE AMERICAN CHEMICAL SOCIETY
pubs.acs.org/JACS
Article

Hybridization from Guest–Host Interactions Reduces the Thermal Conductivity of Metal–Organic Frameworks

Mallory E. DeCoster, Hasan Babaei, Sangeun S. Jung, Zeinab M. Hassan, John T. Gaskins, Ashutosh Giri, Emma M. Tiernan, John A. Tomko, Helmut Baumgart, Pamela M. Norris, Alan J. H. McGaughey, Christopher E. Wilmer, Engelbert Redel, Gaurav Giri, and Patrick E. Hopkins*

Cite This: J. Am. Chem. Soc. 2022, 144, 3603–3613

ABSTRACT: We experimentally and theoretically investigate the thermal conductivity and mechanical properties of polycrystalline HKUST-1 metal–organic frameworks (MOFs) infiltrated with three guest molecules: tetracyanoquinodimethane (TCNQ), 2,3,5,6-tetrafluoro-7,7,8,8-tetracyanoquinodimethane (F_4-TCNQ), and (cyclohexane-1,4-diylidene)dimalononitrile (H_4-TCNQ). This allows for modification of the interaction strength between the guest and host, presenting an opportunity to study the fundamental atomic scale mechanisms of how guest molecules impact the thermal conductivity of large unit cell porous crystals. The thermal conductivities of the guest@MOF systems decrease significantly, by on average a factor of 4, for all infiltrated samples as compared to the uninfiltrated, pristine HKUST-1. This reduction in thermal conductivity goes in tandem with an increase in density of 38% and corresponding increase in heat capacity of ∼48%, defying conventional effective medium scaling of thermal properties of porous materials. We explore the origin of this reduction by experimentally investigating the guest molecules' effects on the mechanical properties of the MOF and performing atomistic simulations to elucidate the roles of the mass and bonding environments on thermal conductivity. The reduction in thermal conductivity can be ascribed to an increase in vibrational scattering introduced by extrinsic guest-MOF collisions as well as guest molecule-induced modifications to the intrinsic vibrational structure of the MOF in the form of hybridization of low frequency modes that is concomitant with an enhanced population of localized modes. The concentration of localized modes and resulting reduction in thermal conductivity do not seem to be significantly affected by the mass or bonding strength of the guest species.

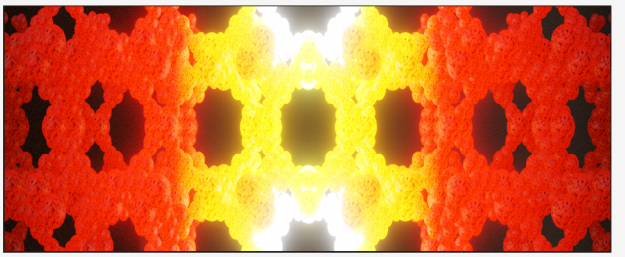

1. INTRODUCTION

Metal–organic frameworks (MOFs) are a class of porous crystalline materials composed of a network of metal ions connected to organic "linker" molecules by coordination bonds. MOFs have a vast variety of applications including gas storage, separation, catalysis, and recently, thermoelectrics (TE).[1−5] Their versatility stems from highly selective chemical and mechanical modifications that are achieved by choice of MOF building blocks (the metal node and ligand), their extremely high porosity/surface area ratio, and the ability to introduce specific guest molecules into the pores of the framework.[2,3,6−8] In particular, tailoring of emergent properties such as electrical conductivity and thermopower has been achieved by infiltrating MOF pores with specialized guest molecules.[2−4] While the thermal properties of MOFs have been investigated on idealized structures using molecular simulations,[9−12] experimental inquiry of infiltrated MOFs is deficient and critically important for realizing efficient gas adsorption and thermoelectric materials.[2,3,13−15] Gas adsorption is an exothermic process, where the desorption entropy results in a decrease in guest material uptake with temperature. Therefore, a guest–host-induced change in the thermal conductivity upon sorption will control the achievable concentration of gas storage available to a MOF material. Additionally, MOFs are a very good candidate as a TE material due to their intrinsic porosity and therefore intrinsically low thermal conductivity and emergent electrical properties upon infiltration with a guest molecule, e.g., TCNQ. Specifically, significantly enhanced charge transport has been achieved upon infiltration of an electrically conductive guest molecule into the pores.[3,4] Understanding the role of guest species on the thermal transport properties of porous crystals, such as MOFs, is critical for informing other chemical properties of the system and is therefore a crucial property for realizing novel and efficient TE and gas storage materials.[4,13]

Received: November 29, 2021
Published: February 18, 2022

https://doi.org/10.1021/jacs.1c12545
J. Am. Chem. Soc. 2022, 144, 3603−3613

In a porous crystal containing adsorbed guest molecules, there are, in general, two main mechanisms that influence the overall heat transfer. These are the thermal transport through the solid scaffolding and through the guest, which are mediated by the guest−host interactions.[16] While MOFs can be modestly electrically conductive,[17] the primary energy carriers are vibrational modes since the electrical conductivity is too low to make any substantial contribution to thermal conductivity.[18] Thermal transport through the guest−host interaction is complex and not well understood because competing effects can impact the thermal conductivity. For example, an effective medium approximation suggests that MOF infiltration should increase the total thermal conductivity since an adsorbed molecule increases the number of atoms per unit volume, serving to increase the density while enhancing the total number of channels that heat can flow through the material system. Alternatively, the addition of any extrinsic species in the form of a guest molecule within the pore could promote a break in the symmetry/periodicity in the crystal and lead to the hybridization of low frequency modes promoting increased scattering and/or changes in mode character (i.e., loss of plane wave/propagating character), which would imply a reduction in thermal conductivity.[18,19] Further, in this picture, the guest molecules can also be thought of as "rattling" atoms that produce strong localized modes that may scatter with MOF vibrational modes, decreasing heat transfer.[20,21] In short, the physical mechanisms driving heat flow processes in porous crystalline material undergoing infiltration require additional examination.

This work experimentally investigates the effects of infiltration of charge accepting guest molecules with differing degrees of orbital overlap between the infiltrated guest and MOF host lattice on the thermal conductivity of HKUST-1. Our experimental results of thermal conductivity of the various MOF samples are supported by molecular dynamics (MD) simulations, MD-derived spectral energy density (SED) calculations, and harmonic lattice dynamics (LD) to elucidate the role of the guest−host interaction on thermal transport processes. HKUST-1 is a common, easily fabricated MOF constructed from metal nodes of dimeric Cu^{2+} paddle-wheel units, where each Cu atom is coordinated by four oxygens from the benzene-1,3,5-tricarboxylate (BTC) linkers, forming face centered-cubic (fcc) crystals.[22−24] HKUST-1 contains a three-dimensional network of periodic square-shaped pores (9 × 9 Å) with varying levels of polarity based on their exposure to the metallic coordinatively unsaturated site (CUS).[25,26] Molecular structures of the HKUST-1 building block and guest molecules are detailed in Figure 1. Before infiltration, the HKUST-1 pristine framework is an insulator that is electrically neutral; it has a partially positive charge on the Cu^{2+} atoms that is balanced by the partially negative localized charge on the carboxylate units within the BTC linker of the polymeric crystal lattice.[27] For the purposes of this study, HKUST-1 is infiltrated with three charge-accepting molecules, listed here in order of decreasing guest−host bond overlap: tetracyanoquinodimethane (TCNQ), 2,3,5,6-tetrafluoro-7,7,8,8-tetracyanoquinodimethane (F_4-TCNQ), and (cyclohexane-1,4-diylidene)dimalononitrile (H_4-TCNQ). These guest molecules have previously been shown to enhance the electrical conductivity of the guest@MOF system by more than 6 orders of magnitude by introducing covalent and noncovalent interactions that create continuous charge transport pathways through long-range order of the donor bridge acceptor sites

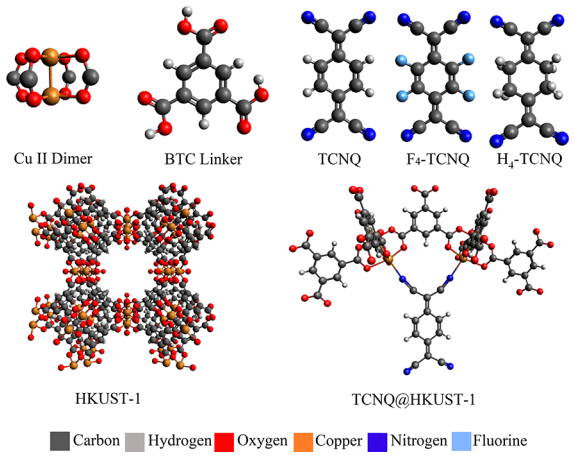

Figure 1. Schematic of the building blocks and guest molecules of the guest@HKUST-1 system: (top) Cu(II) dimer metal node (note that the Cu(II) paddle-wheel dimer shows the Cu^{2+} coordinated to eight oxygens from four separate BTC molecules), BTC linker, and the TCNQ, F_4-TCNQ, and H_4-TCNQ guest molecules. (Bottom) the full assembly of a single unit cell of the pristine HKUST-1 is shown along with a zoomed-in representation of the TCNQ@HKUST-1 bonding environment as described by Allendorf *et al.*[3]

and mixing between the electronic excited and ground states.[1,3] It is important to note, however, that the electrical conductivity of the guest@HKUST-1 is still relatively low, which is quite detrimental toward its application as a thermoelectric material. TCNQ, F_4-TCNQ, and H_4-TCNQ are strong π-acids that accept electrons from the Cu(II) dimers of the HKUST-1. Talin *et al.* showed that loading of the TCNQ guest species into HKUST-1 results in approximately eight molecules per unit cell, or one molecule per pore.[4] Additionally, there exists strong evidence of coordination occurring between the terminating nitrile groups of TCNQ (which are *cis* to each other) and the CUS of the MOF, where this interaction is thought to be responsible for the emergence of electronic conductivity upon infiltration (Figure 1).[3] Since the degree of charge transport is closely related to the crystal binding energy, we use the predicted metric for donor/acceptor electronic coupling from Allendorf *et al.* to qualitatively rank the degree of guest−host orbital overlap between each guest species.[3] TCNQ provides the largest coupling with the MOF owing to a high degree of orbital overlap between the TCNQ and the Cu d(z^2) orbitals within the metal node of the MOF. Fluorination of TCNQ results in added tuning, where an increase in electronegativity causes an overall reduction in electrical conductivity by disrupting the d orbital overlap between the guest and host.[3] Last, H_4-TCNQ produces the least charge transport of all guest molecules, due to the lack of a conjugated π network, and therefore has the smallest orbital overlap.

To support the thermal conductivity measurements, we extensively characterize surface-anchored metal−organic framework (SURMOF) thin films (250−400 nm) and thick polycrystalline samples (5.5 μm) of pristine and infiltrated HKUST-1 with scanning electron microscopy (SEM), X-ray diffraction (XRD), infrared spectroscopy, nuclear magnetic resonance spectroscopy (NMR), pump-probe Brillouin scattering, and nanoindentation (Figure 3 and Sections S1, S2, and S5−S10) to examine the structural properties and coordination environment. Pump-probe Brillouin scattering and nanoindentation measurements demonstrate the role of infiltration

https://doi.org/10.1021/jacs.1c12545
J. Am. Chem. Soc. 2022, 144, 3603−3613

on the elastic modulus of the MOF samples, which further elucidates the fundamental role of guest−host interactions on the stiffnesses of the MOFs. Further, we offer an interpretation of our experimental results with atomistic MD, SED, and LD simulations to ascertain the guest−host interactions on thermal conductivity, vibrational modes, and scattering rates. Due to the complex interplay of order and disorder in these large unit cell crystals with addition of a guest, we frame our interpretation of the simulated and experimental results from a disordered framework perspective. We presume that a combination of extended (phonon-like propagating modes known as propagons and non-propagating diffusons) and localized (locons) modes are present in our MOF systems.[18,28,29] We find that the thermal transport in these infiltrated porous crystalline systems is not influenced by a loading-dependent structural change but rather an increase in extrinsic vibrational scattering introduced by guest-MOF collisions as well as adsorbate-induced modifications to the vibrational structure resulting in hybridization with low frequency modes and a concomitant increase in mode localization. The infiltrated MOF materials have a higher degree of localized modes at all frequencies than the uninfiltrated pristine states that are not significantly affected by the mass or bonding strength of the guest species.

2. RESULTS AND DISCUSSION

SURMOF thin film and thick polycrystalline HKUST-1 MOFs were prepared at two separate institutions, Karlsruhe Institute of Technology (KIT) and the University of Virginia (UVA), using a layer-by-layer (LBL) liquid phase epitaxy (LPE) technique[30] and a solution shearing[31−33] fabrication process, respectively. These methods are described in detail in the Experimental Section. All pristine samples were activated by heating at 145 °C for 12 h under a vacuum of 3.4×10^{-6} mbar, which has been shown to be an effective technique to remove both pre-coordinating solvent molecules and unwanted guest molecules, such as H_2O and CO, that would otherwise prevent the pores from interacting with the intended adsorbates while maintaining the crystallinity and porosity.[24,34,35] Activation immediately before measurement acquisition of the pristine HKUST-1 is a crucial step for realizing a truly pristine HKUST-1 sample, where upon deactivation, water vapor adsorbed into the pores causes a reduction in the thermal conductivity (Figure S9). Pristine HKUST-1 samples were exposed to a saturated solution of TCNQ, F_4-TCNQ, and H_4-TCNQ, the details of which are provided in the Experimental Section, to provide a series of pristine and infiltrated HKUST-1 samples. We measured the thermal conductivities of the various HKUST-1 SURMOF films and thick samples in activated pristine and loaded forms with time domain thermoreflectance (TDTR).[36,37] We experimentally modify the strength of the coordination between the guest and host by choosing a fluorinated (F_4-TCNQ) and a hydrogenated (H_4-TCNQ) equivalent to the TCNQ molecule, which adjusts the degree of orbital overlap between the nitrile functional group from the guest and Cu^{2+} d orbital from the host and alters the extent of electronic coupling.[38,39]

Figure 2 shows the measured thermal conductivity as a function of thickness for activated pristine and infiltrated samples. The previously reported literature value for the thermal conductivity of TCNQ@HKUST-1 from Erickson *et al.*[2] of 0.27 ± 0.04 Wm^{-1} K^{-1} is also shown for reference; our results for the infiltrated MOFs are in agreement with this

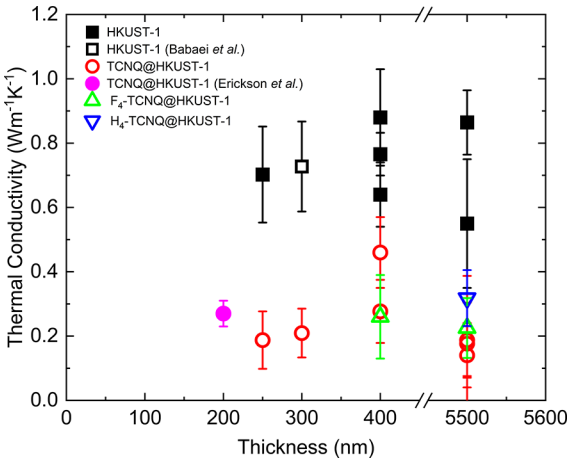

Figure 2. Experimentally measured thermal conductivity vs thickness of activated pristine HKUST-1 (black filled squares) and infiltrated HKUST-1 (open symbols). The reported measured thermal conductivity of a 200 nm-thick film of TCNQ@HKUST-1 (pink filled circle) from Erickson *et al.*[2] and a 300 nm pristine HKUST-1 film (black open square) from our previous work[13] are also shown for reference. Table S1 lists details on the individual samples.

reported value. We note that Erickson *et al.*[2] used MD to show that the addition of TCNQ significantly increases the thermal conductivity, while we show experimentally that infiltration with TCNQ significantly decreases the thermal conductivity of the HKUST-1 system. The discrepancy likely lies in the assumptions made in the MD. Primarily, Erickson *et al.* modeled the TCNQ molecules with non-bonding interactions with the framework so that the TCNQ molecules' main function was to provide structured additions (increased density) to the framework. As shown from our characterization data (Figure 3) and reported elsewhere,[3,4,40] it is more likely that the TCNQ coordinates with the framework and therefore behaves very differently (phonon scatterers) than what was captured by Erickson *et al.* Returning to our experimental results, the lack of dependence of the thermal conductivity on sample thickness suggests that the mean free paths of the heat-carrying propagons are much less than the film thicknesses or grain sizes (~300 nm, confirmed from XRD (see Section S1)), which is consistent with prior reports on the mean free paths in these systems.[11,41] Additionally, the lack of a classical size effect also indicates that the dominant vibrational modes that contribute to the thermal conductivity of the material may be non-propagating (e.g., diffusons).[18,42]

In our experimental geometry, TDTR is primarily sensitive to the thermal effusivity ($\sqrt{\kappa C_v}$) of the sample (except for the thinnest 250 nm SURMOF HKUST-1 sample, where TDTR is sensitive to both thermal conductivity and heat capacity simultaneously, as we discuss in Section S3, where the thermal conductivity (κ) is the fitting parameter and the volumetric heat capacity (C_v) is taken as a known parameter (either measured or obtained from the literature,[2] see Section S3). Effective medium theory would predict that an increase in the density of the material (upon loading) would result in an increase in the thermal conductivity due to an increase in the density of the porous composite. We measure a decrease in the thermal effusivity upon loading, indicating that the drastic drop in thermal conductivity cannot be explained by the increase in the density or volumetric heat capacity. This finding implies a more complex heat transfer picture where the adsorbate

https://doi.org/10.1021/jacs.1c12545
J. Am. Chem. Soc. 2022, 144, 3603−3613

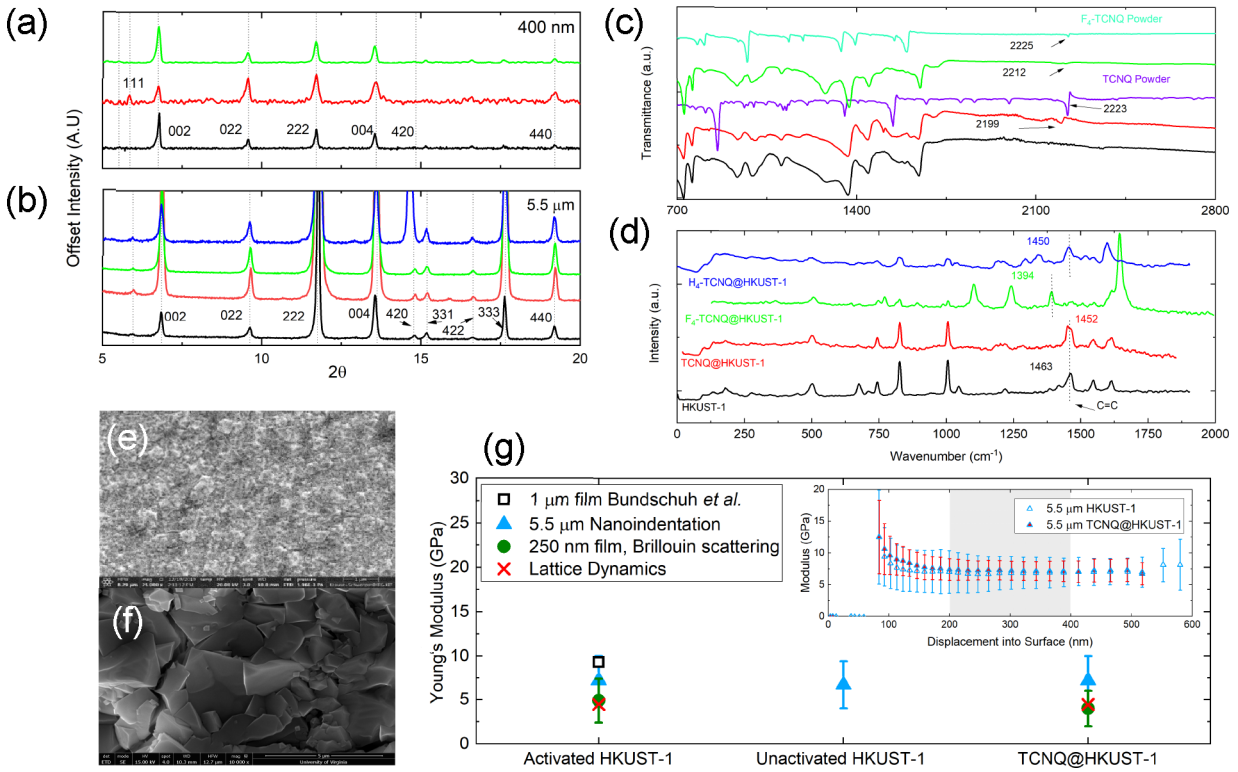

Figure 3. Characterization of samples. (a) XRD data for F_4-TCNQ@HKUST-1 (green), TCNQ@HKUST-1 (red), and HKUST-1 (black) 400 nm thin films and (b) XRD for the H_4-TCNQ@HKUST-1 (blue), F_4-TCNQ@HKUST-1 (green), TCNQ@HKUST-1 (red), and HKUST-1 (black) 5.5 μm-thick MOF samples. We see little evidence of excess TCNQ, F_4-TCNQ, and H_4-TCNQ that did not diffuse into the pores. (c) FTIR spectra for 5.5 μm-thick pristine (black), TCNQ@HKUST-1 (red), and F_4-TCNQ@HKUST-1 (green) MOFs compared to TCNQ (purple) and F_4-TCNQ (aqua) molecules in powder form. The respective nitrile stretch is labeled in the spectra, and the magnitude of the red shift occurring from the guest species in powder form to infiltrated form shows the degree that the TCNQ/F_4-TCNQ interacts with the coordination sites of the framework. (d) Raman spectra for the 5.5 μm-thick pristine (black), TCNQ@HKUST-1 (red), F_4-TCNQ@HKUST-1 (green), and H_4-TCNQ@HKUST-1 (blue) MOFs. The C═C stretching frequency is labeled. The shift of the C═C stretching frequency upon infiltration and the additional peaks occurring between 1101 and 1343 cm^{-1} indicate that the TCNQ and F_4/H_4-TCNQ derivatives coordinate to the Cu^{2+} ions in the framework. (e) Planar SEM images for the 400 nm pristine polycrystalline HKUST-1 SURMOF thin films fabricated by LBL-LPE from KIT and (f) 5.5 μm-thick polycrystalline HKUST-1 samples fabricated using solution shearing at UVA. (g) Young's Modulus for 400 nm and 5.5 μm pristine and TCNQ@HKUST-1 samples measured by pump-probe Brillouin scattering and nanoindentation, respectively. The results are compared to the lattice dynamics-derived Young's Modulus using a Poisson ratio of 0.49 and also to nanoindentation results for a 1 μm HKUST-1 film from Bundschuh *et al.*[43] The inset shows the full range of indenter displacement on the 5.5 μm pristine and TCNQ@HKUST-1 samples; however, only data in the shaded region were used for analysis.

introduces disorder into the system. In fact, previous molecular dynamics studies on liquid- and gas-loaded MOF systems have reported similar thermal trends, concluding that the reduction in κ upon infiltration is due to higher vibrational scattering rates introduced by the collisions between gas molecules and the MOF lattice sites.[10,13] Note that the results for thin film H_4-TCNQ@HKUST-1 are not reported in Figure 2 due to procedural difficulties in achieving successful diffusion of the highly volatile H_4-TCNQ molecule into the HKUST-1 pores (see Section S1 for details).

Previously, we experimentally observed a characteristic decrease in the thermal conductivity of HKUST-1 SURMOF films and single crystals upon infiltration with methanol, ethanol, and water.[13] Prestipino *et al.* have shown that H_2O molecules present in the pores of HKUST-1 chemically bind to the Cu(II) sites, resulting in significant modifications to the first coordination sphere,[24] which structures a hypothesis of the fundamental chemical nature of the infiltrated species-MOF interaction that can reduce the thermal conductivity of guest@MOFs. Specifically, hydration results in the distortion of the intrinsic Cu−O bonds in the Cu(II) dimer and lengthening of the Cu−Cu distance, resulting in an overall increase in cell volume. It is likely that the introduction of the other polar liquid guest molecules (methanol and ethanol) in our previous work created similarly complex guest−host interactions. We can translate this discussion to posit the fundamental chemical interactions between the guest molecules and HKUST-1 cages that drive down the thermal conductivity in the materials studied in this work. Figure 3 shows characterization data for the thin and thick MOFs, including SEM, XRD, FTIR, Raman, and nanoindentation paired with pump-probe Brillouin scattering measurements of the elastic modulus (see Sections S1, S2, S5, S6, S9, and S10 for full details) that specify the morphology of each sample and confirm the presence of different degrees of guest coordination with the framework. The XRD and SEM data shown in Figure 3a,b and Figure 3e,f, respectively, show that the surface-anchored thin films exhibit low surface roughness and highly oriented growth. This is in contrast to the thick MOFs, which demonstrate elevated surface roughness and high polycrystallinity. The SEM in Figure 3e,f shows the difference in surface roughness, where the LPE method produces very low

https://doi.org/10.1021/jacs.1c12545
J. Am. Chem. Soc. 2022, 144, 3603−3613

surface roughness (<10 nm) and the solution shearing method promotes high surface roughness (~1 μm), as confirmed through profilometry. Further, the XRD in Figure 3a,b confirms that infiltration does not affect the MOF's crystalline structure (fcc). Additionally, it has been reported that the XRD peak occurring at $2\theta \simeq 5.7$ is a diagnostic for the guest molecules binding to the open metal sites of the framework.[4] Indeed, Figure 3b shows the emergence of a peak at $2\theta \simeq 5.9$ in the infiltrated cases for the thick MOFs that is absent for the pristine HKUST-1 samples. We note that the LBL-created SURMOF TCNQ@HKUST-1 thin films show a feature at $2\theta \simeq 5.87$; however, this feature is quite weak in the F_4-TCNQ@HKUST-1 diffractogram. The FTIR spectra for powder forms of TCNQ and F_4-TCNQ are compared to the infiltrated forms (TCNQ/F_4-TCNQ@HKUST-1) and the pristine MOF in Figure 3c. The red shifts of the nitrile peak of 13 cm^{-1} for F_4-TCNQ/F_4-TCNQ@HKUST-1 (from 2225 to 2212 cm^{-1}), 24 cm^{-1} for TCNQ/TCNQ@HKUST-1 (from 2223 to 2199 cm^{-1}), and broadening of the nitrile stretch indicate the degree that the guest molecules are interacting with the coordinating Cu^{2+} sites of the paddle-wheel units in the framework.[4] Further, the Raman spectra in Figure 3d from the thick samples show that the bonding environment within the pore between the TCNQ, F_4-TCNQ, and H_4-TCNQ is quite different from species to species, where new features appear in the F_4-TCNQ, and H_4-TCNQ infiltrated MOFs that are not present in the TCNQ system (see Section S5 for full details). Moreover, the feature at ~507 cm^{-1} that represents the Cu−O stretch is blue-shifted (higher energy) for the F_4-TCNQ and broadened in the H_4-TCNQ spectrum, demonstrating different interactions of the guest molecule in the first coordination sphere of the Cu^{2+} sites. The aromatic alkene (C═C) stretch at ~1463 cm^{-1} is red-shifted for the infiltrated guests, which is also strong evidence of guest coordination with the MOF.[4] We note that others have also reported coordination occurring between the TCNQ and TCNQ derivatives with the CUS of HKUST-1.[3,4,40]

Mechanical measurements of the elastic constants of pristine (in activated and unactivated forms) and TCNQ infiltrated HKUST-1 using nanoindentation and pump-probe Brillouin scattering are reported in Figure 3g and compared to our harmonic lattice dynamics calculations and previous nanoindentation results from the 1 μm surface-anchored HKUST-1 film prepared using LPE from Bundschuh *et al.*[43] The full details of this analysis can be found in the Supporting Information (Sections S9 and S10). The experimental and lattice dynamics results presented here indicate that no discernable change in Young's modulus is observed between the pristine HKUST-1 and infiltrated TCNQ@HKUST-1 within uncertainty. We note that both an increase in the density of the system due to the presence of guest molecules and an increase in guest−host bonding would typically lead to an increased degree of resistance toward deformation (increased elastic constants). Instead, no measurable change is observed, suggesting that the unit cell deformation upon infiltration/adsorption may compete with density and bonding effects. We conclude from these measurements that mechanical softening upon infiltration of HKUST-1 is negligible, and therefore, a loading-dependent structural change can be ruled out from contributing to the reduction in the thermal conductivity.

A guest molecule-induced thermal conductivity reduction appears in all guest−host bonding environments (Figure 2). We turn to MD simulations and SED analysis to resolve the effects of bonding morphology (orientation and number) on this observed reduction in thermal conductivity and vibrational scattering. Allendorf *et al.* proposed that each TCNQ within a pore likely forms two covalent bonds once infiltrated, occurring between two *cis* terminating nitrile groups and the Cu(II) dimers within the coordinated unsaturated sites (CUS) (Figure 1).[3] Others have identified other possible phases of TCNQ within HKUST-1 including a neutral and dimeric species that do not coordinate to the open Cu^{2+} sites.[40] The diffusion of F_4/H_4-TCNQ in HKUST-1 pores has not been as thoroughly investigated. These previous works help to inform the likely morphology of the infiltrated films, yet there still remains uncertainty in how different variations in the concentration and bonded orientation of guest molecules within pores will affect the thermal conductivity of the guest@MOF system.

Therefore, we perform MD simulations by varying the number of bonds and concentration of guest molecules to investigate the effect of bonding morphology of the guest molecule on the thermal properties. Figure 4a−c illustrates the different bonding nature of the systems studied via MD. We performed simulations with TCNQ infiltrated in three different states within the MOF pore: formation of two covalent bonds in a *cis* configuration (Figure 4a), four covalent bonds forming a full bridge across the pore (Figure 4b), and an unbonded "free state" (Figure 4c). The concentration of molecules within the pore is also varied from 1 to 10 (see Section S11 for full details). We use the nomenclature "$TCNQ_{n=x,b=y}$@HKUST-1" to indicate the adsorbed bonding conditions, where n is the number of TCNQ molecules per pore and b is the number of covalent bonds formed with the host ($b = 0$ indicates an unbound free state). We estimate that our experimental results resemble the "$n = 1$, $b = 2$" MD case; however, additional phases resembling the "$n = 1$, $b = 0$" and "$n = 2$, $b = 0$" structures have also been reported to exist within the HKUST-1 pore.[40]

The room temperature MD and experimental results plotted in Figure 4d for the morphological study of guest−host interactions show a reduced thermal conductivity upon all loading cases. In MD, the greatest reduction occurs for the highest TCNQ loading density in an unbound state, and the smallest reduction occurs for a single TCNQ molecule bonded on all sides by all four terminating nitrile groups. In the former case, non-bonded TCNQ molecules are free to collide with the framework and scatter vibrational modes, resulting in the greatest reduction. A larger number of guest molecules result in increased reduction as there are a higher frequency of adsorbate- framework collisions. In the latter case, the TCNQ is more sterically hindered and oriented within the pore, forming a "thermal bridge", which results in new heat transfer pathways that compete with the vibrational scattering introduced by the guest, resulting in the smallest overall reduction in thermal conductivity. The intermediate cases involve the TCNQ bonded on one side to the pore ($b = 2$), where the TCNQ can still rattle but has less freedom to collide with the adsorbate framework. Without any direct evidence for the bonding experienced by the polar liquid guest molecules within the HKUST-1 pores, we also compare the mass effects of the guests, including the liquid polar guest molecules from our previous study,[13] to the total thermal conductivity of the infiltrated MOF system by plotting the experimentally obtained thermal conductivity to the molecular weight of the

https://doi.org/10.1021/jacs.1c12545
J. Am. Chem. Soc. 2022, 144, 3603−3613

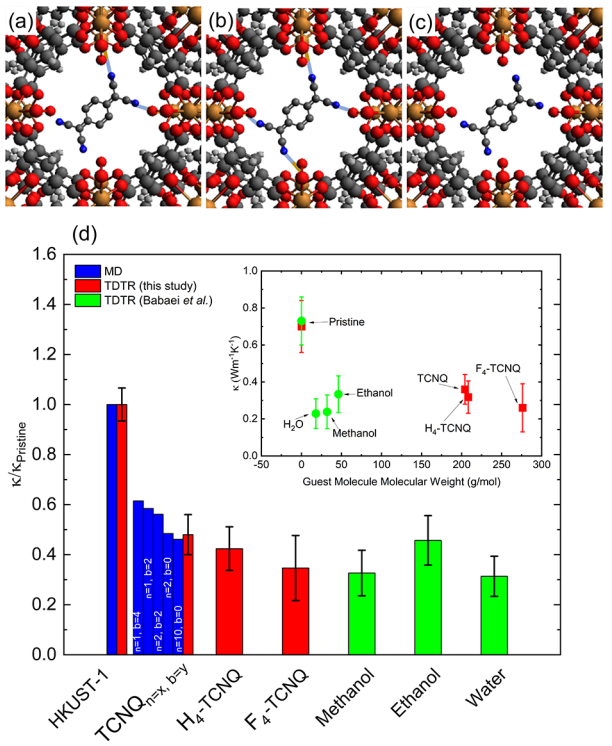

Figure 4. (a–c) Visualizations of the infiltrated pore bonding morphologies considered for MD simulations. The nomenclature "$TCNQ_{n=x,b=y}$@HKUST-1" indicates the adsorbed bonding conditions, where n is the number of TCNQ molecules per pore and b is the number of covalent bonds formed between the guest and host ($b = 0$ indicates the unbound free state). (a) Two covalent bonds on one side (*cis* to each other) of a single TCNQ molecule ($n = 1$, $b = 2$), (b) a single TCNQ that creates four covalent bonds with the host ($n = 1$, $b = 4$), and (c) a single unbonded free state TCNQ molecule ($n = 1$, $b = 0$). The concentration of molecules within the pore is varied from 1 to 10. (d) Normalized room temperature thermal conductivity comparing the MD (blue) to the TDTR measured results for HKUST-1 and guest@HKUST-1 from this study (red) and our previous study (green).[13] All thermal conductivities have been normalized to the thermal conductivity of the pristine HKUST-1 ($\kappa_{Pristine}$). We note that the experimental data for the 400 nm thin films are shown for TCNQ and F_4-TCNQ, while the H_4-TCNQ results are from the 5.5 μm-thick samples. The HKUST-1 samples infiltrated with methanol, ethanol, and water were 200 nm thick and are from our previous work (green).[13] The inset shows the experimentally measured thermal conductivity for the guest molecules as a function of molecular weight.

guest molecule (Figure 4d, inset). The heaviest guest (F_4-TCNQ) is over an order of magnitude heavier than the lightest guest (H_2O). We note that the liquid guests fill the pores of HKUST-1 with a liquid void fraction between 82 and 100% (~120 molecules per pore), and the TCNQ guests average one molecule per pore.[4,44] The experimental results for the solid TCNQ and TCNQ analogue guest molecules compared to the liquid polar guests (methanol, ethanol, and water) studied previously do not show the emergence of an obvious guest-dependent thermal trend; however, it is possible that the effects of bonding morphology revealed from MD may fall within the uncertainty of our experimental measurements. The MD and experimental results show a decrease in thermal conductivity upon infiltration, and neither the mass nor the bonding morphology of the guest suitably predicts the magnitude of the reduction.

MD-derived SED calculations were performed in the [100] crystallographic direction and helped to elucidate the role of scattering of low frequency vibrational modes introduced by the guest molecules. SED demonstrates that the vibrational mode lifetimes are reduced in the frequency range of 0–15.3 THz, upon infiltration with TCNQ (Figure 5). We note that vibrational mode lifetimes could not be accurately derived above ~3 THz and below ~15.3 THz due to the lack of clearly defined peaks in this regime (see Section S13). Figure 5 shows that the high frequency modes (>15.3 THz) are relatively unaffected by adsorption; however, the lifetimes for the low frequency modes (0.5–15 THz) are greatly affected by the presence of TCNQ. The long lifetimes of the low frequency modes in the pristine HKUST-1 indicate that these modes carry the majority of heat at room temperature and are responsible for the large reduction in thermal conductivity upon guest adsorption measured experimentally. Figure 5 also shows that vibrational lifetimes $\lesssim$15.3 THz of the TCNQ in a bonded orientation result in shorter lifetimes than in the pristine MOF, and the effects of the free TCNQ pore orientation are so drastic that the peaks disappear (i.e., no modes exist). In total, the MD and SED suggest that extrinsic adsorbate-MOF collisions increase scattering rates of extended vibrational modes to drive down the thermal conductivity, where an unbound adsorbate is more effective than a bonded adsorbate in diminishing these vibrational mode lifetimes. Figure 4d shows that the experimentally measured thermal conductivities of the TCNQ and TCNQ analogue-infiltrated MOFs more closely resemble the "$b = 0$" MD cases, although their bonding morphology is expected to resemble "$b = 2$".[3] This suggests that, while extrinsic adsorbate/MOF collisions likely play a significant role in diminishing the thermal conductivity, the role of the bond between the adsorbate/MOF may not produce a competing thermal bridge effect as suggested by the MD. Instead, it may further aid in reducing the thermal conductivity by changing the vibrational structure via intrinsic mechanisms (i.e., hybridizations).

To investigate the role of the adsorbate bond on the vibrational structure of HKUST-1, we performed harmonic lattice dynamics, which captures the effects of bond strength of the guest–host interaction. The infiltrated cases modeled here are similar to the "$n = 1$, $b = 2$" case modeled in MD. We reiterate that the infiltrated MOFs are crystalline systems that contain intrinsic disorder stemming both from the introduction of guest molecules and from their large unit cells. In particular, a large number of atoms in the unit cell can result in low lying optical modes that are close to the acoustic modes, which produce an increased phase space for scattering events that promotes reduced vibrational mode lifetimes.[45,46] Indeed, the LD-derived dispersions show evidence of low lying optical propagons and avoided crossings occurring in the infiltrated HKUST-1 systems studied here (see Section S12). Additionally, the trend in lifetimes captured by SED (Figure 5, inset) shows that the thermal transport in pristine HKUST-1 can be described by a propagon–diffuson picture and the addition of a guest adds disorder, which breaks the crystal periodicity and creates locons to reduce the thermal conductivity. Therefore, we offer an interpretation of the heat transport in these partially disordered materials by calculating the inverse participation ratio (IPR), which provides insight into how vibrational modes with different frequency and localization characteristics contribute to thermal conductivity.[47] Additionally, the Allen–Feldman (A-F) method for calculating thermal

https://doi.org/10.1021/jacs.1c12545
J. Am. Chem. Soc. 2022, 144, 3603–3613

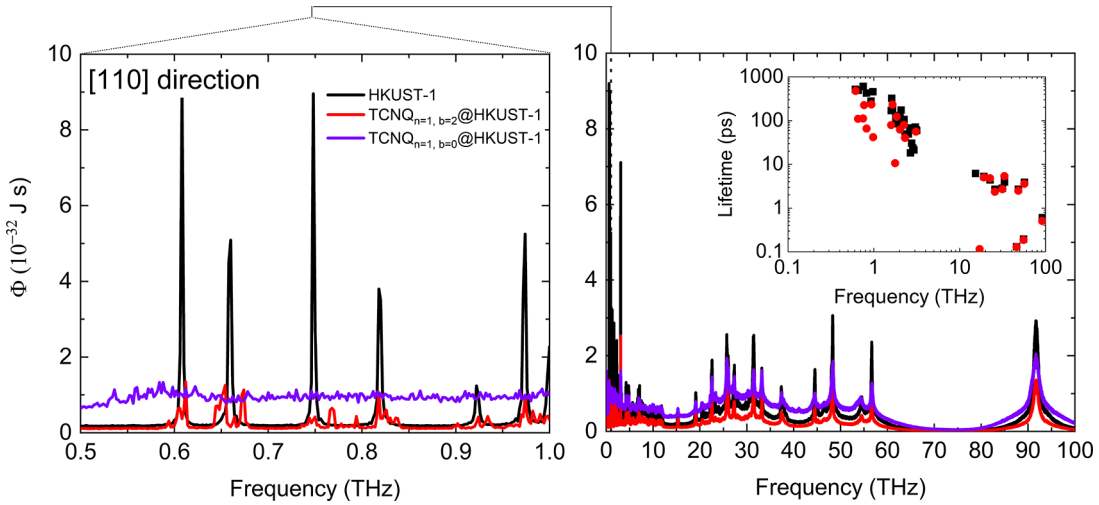

Figure 5. Spectral energy density (SED) results of pristine HKUST-1 (black) and TCNQ@HKUST-1 infiltrated under two different bonding conditions, bonded (red) and unbonded (purple), calculated for the {100} crystallographic direction only, where Φ is a representation of the vibrational energy in the frequency domain. The right panel shows the full spectrum of modes, and the left panel shows a zoom in from 0.5 to 1 THz. The inset shows the corresponding vibrational mode lifetimes. In the pristine case, many sharp peaks are observed at lower frequencies (left panel) that indicate vibrational modes with long lifetimes. The lifetimes of the low frequency modes in the TCNQ$_{a\ =\ 1,b\ =\ 2}$@HKUST-1 are significantly reduced. In comparison, the higher frequency modes above ∼15.3 THz in the pristine case have much shorter lifetimes and therefore do not contribute as much to heat transport. Additionally, we do not see any associated lifetime changes in the pristine case compared to the bonded infiltrated case for the high frequency modes (see Section S13 for more details).

conductivity also provides insight in the limit where vibrational modes are defined as diffusons.[48]

Figure 6a shows the vibrational density of states (DOS) for the pristine and TCNQ infiltrated HKUST-1 and a single isolated TCNQ molecule. The emergence of a new population of localized modes within the TCNQ@HKUST-1 system is clear, which evidently corresponds with molecular modes intrinsic to the single TCNQ molecule.[10,43,44] To understand the effect of this new population of modes, we calculate the IPR, which conceptualizes the concentration and distribution of delocalized extended modes (propagons and diffusons) and localized (locons) modes given by

$$\mathrm{IPR} = \frac{\sum_i^N \left(\sum_{\alpha=1}^3 u_{i\alpha}^2\right)^2}{\left(\sum_{i=1}^N \left(\sum_{\alpha=1}^3 u_{i\alpha}^2\right)\right)^2}$$

where N is the number of atoms (624) and $u_{i\alpha}$ is the eigenvector component for atom i in the direction α.[49] Here, we define locons as vibrational modes whose eigenvectors spread across 20% or less of the atoms in the unit cell (corresponding to 125 atoms, IPR = $1/N \geq 0.008$), which has been shown by others to be a reasonable delineation.[49,50] Figure 6b shows the IPR results calculated for the vibrational modes at the Γ point of the Brillouin zone. The non-propagating modes become increasingly localized in the infiltrated cases, where modes outside of the beige shaded region (IPR ≥0.008) are localized. To quantify these results, we plot the accumulation of the total number of locons at the Γ point as a function of frequency in Figure 6d. In total, the HKUST-1 infiltrated TCNQ and F_4-TCNQ show that 40 and 38% of the modes become localized, respectively, compared to 2% in the pristine HKUST-1, at the Γ point. In particular, a high concentration of localized modes appear between 13 and 32 THz. Together, Figure 6c,d shows that the weaker bonded F_4-TCNQ results in slightly less localized modes than the stronger bonded TCNQ and that low frequency non-propagating modes (<4.65 THz) contribute considerably to the total thermal conductivity of the infiltrated material.

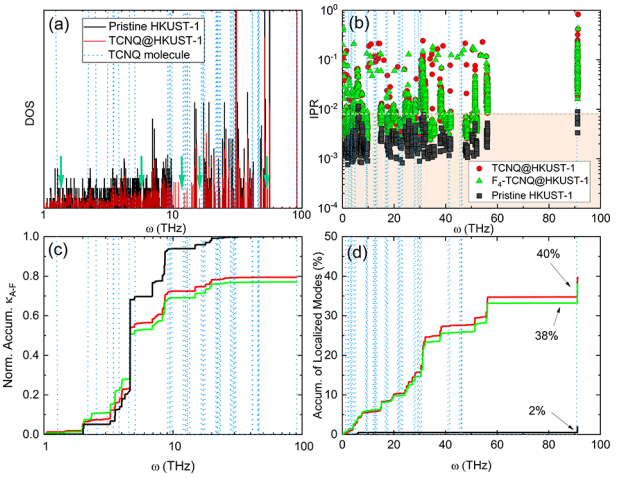

Figure 6. (a) Vibrational density of states (DOS) for the HKUST-1 (black) and TCNQ@HKUST-1 (red) compared to the vibrational spectrum of a single isolated TCNQ molecule (blue dotted lines). The DOS for F_4-TCNQ@HKUST-1 has been left off for clarity. We see the emergence of new modes upon infiltration that overlap with the TCNQ molecular modes (pointed out by the green arrows). (b) Mode-resolved inverse participation ratio (IPR) calculated at the Γ wave vector only. The beige shaded region corresponds to the delocalized modes, where the transition from delocalized to localized modes occurs at an IPR ≥ 0.008, corresponding to eigenvectors that are spread across 20% or less of the atoms in the supercell (125 atoms). (c) Thermal conductivity accumulation from non-propagating modes (diffusons) calculated from Allen−Feldman theory at 300 K normalized to the κ_{A-F} for pristine HKUST-1 and (d) the accumulation of IPR calculated localized modes at the Γ wave vector in pristine HKUST-1 (black), TCNQ@HKUST-1 (red), and F_4-TCNQ@HKUST-1 (green) and an isolated TCNQ molecule (blue dotted lines).

https://doi.org/10.1021/jacs.1c12545
J. Am. Chem. Soc. 2022, 144, 3603−3613

The IPR results (Figure 6b,d) show that the bonded adsorbate contributes to a substantial population of localized modes that span a broad range of frequencies. In particular, these modes are concentrated from 13 to 32 THz, which corresponds to a high degree of overlap with the single isolated TCNQ molecule vibrational spectrum. This result shows that the coordinated guest molecules residing in the pores of the MOF contribute to the reduction of the thermal conductivity of the MOF through two intrinsic mechanisms resulting in a change of the vibrational structure of the MOF. First, the hybridization (i.e., avoided crossings) with propagons will tend to broaden peaks in the vibrational density of states,[51] and such behavior has been shown to significantly reduce the thermal conductivity (though the mechanism is still heavily debated).[41,45] We see evidence of hybridization occurring in the infiltrated systems captured as low lying optical and acoustic coupling in the dispersions and broadening of peaks in the DOS shown in Figure S21. Second, the adsorbates add disorder into the system resulting in a substantial increase in localized incoherent vibrational modes over a broad frequency range, which increases the phase space for scattering events to occur, thus driving down extended vibrational mode lifetimes (Figure 6b,d). The localized modes in the DOS appear as delta functions[51] and are clearly seen from 9.7 to 16.2 THz in Figure 6a, though IPR results indicate that they occur over a broad range of frequencies (Figure 6b,d). The effect of hybridization and localized modes over a broad frequency range is evidence that the coordinated nature of the adsorbate introduces intrinsic effects, which further contributes to the reduction in thermal conductivity of the adsorbate-MOF system.

The effects of non-propagating modes (diffusons) are captured by calculating the normalized thermal conductivity accumulation function from the A-F method.[48] Figure 6c shows the A-F thermal conductivity accumulation normalized to the pristine HKUST-1 thermal conductivity. The results show that low frequency non-propagating modes (0−4.65 THz) contribute to a higher degree to the thermal conductivity for the infiltrated HKUST-1; however, short wavelength modes >4.65 THz participate to a larger degree in the pristine case. This result indicates an increase in the contribution to thermal conductivity of non-propagating modes at frequencies below 4.65 THz when infiltrated; however, we see a reduction in diffuson contribution at higher frequencies, which is consistent with the frequency distribution of the new population of locons identified by the IPR. Note that the contribution of propagons is not included in the A-F thermal conductivity approach. In total, the A-F-derived thermal conductivities show a reduction in thermal conductivity for both the TCNQ and F_4-TCNQ infiltrated systems (21% and 24%, respectively), where varying the bond strength of the guests to the host lattice by ∼8% and the mass of the guest atom by 35% leads to only an ∼3% difference in the thermal conductivity between the lighter stronger bonded TCNQ and the heavier weaker bonded F_4-TCNQ guest molecules. This indicates that the guest−host bond strength does not greatly affect the thermal conductivity reduction.

3. CONCLUSIONS

Metal−organic frameworks offer a unique system to study the thermal properties of periodic porous materials in pristine and adsorbed states. We measure the thermal conductivity of SURMOF thin films and thick polycrystalline HKUST-1 fabricated via LBL-LPE and solution shearing, respectively, infiltrated with TCNQ, F_4-TCNQ, and H_4-TCNQ that produce decreasing degrees of coordination to the MOF host framework. We find that the thermal and mechanical properties of the thin and thick samples are consistent despite very different fabrication techniques and locations. Upon infiltration with solid electrically conductive guest molecules, the thermal conductivity decreases by, on average, a factor of 4 for all infiltrated samples studied in this work, as compared to the pristine HKUST-1. The reduction in thermal conductivity is due to both extrinsic and intrinsic effects of the adsorbate. The presence of the adsorbate in the pore results in adsorbate/MOF collisions that serve to extrinsically increase vibrational scattering rates. Additionally, the coordinated guest also modifies the vibrational structure of the MOF through hybridization of modes, which reduces vibrational lifetimes and also contributes to a change in the vibrational mode character by promoting an increase in localized incoherent modes over a broad range of frequencies. In total, our experimental and LD results show that the degree of orbital overlap does not greatly affect the degree of thermal conductivity reduction experienced upon guest adsorption.

We experimentally and theoretically investigated the role of coordination (by choosing guests that produce varying degrees of orbital overlap with the MOF) and composition of guests introduced to the HKUST-1 pore. The MD simulations revealed that the bonding morphology (i.e., bond concentration and orientation) may play the largest role in predicting the magnitude of reduction in thermal conductivity, where an unbonded guest molecule that can collide with the pore wall may produce the largest reduction, and bonds formed between the guest/host can serve to compete with scattering processes by acting as thermal bridges. However, our experimental and LD results indicate that guest-MOF bonding serves to enhance rather than hinder vibrational scattering rates by promoting changes to the vibrational structure of the MOF via hybridization.

4. EXPERIMENTAL SECTION

4.1. Liquid Phase Epitaxy of Thin Film HKUST-1. Polycrystalline HKUST-1 surface-anchored MOF (SURMOF) thin films were self-assembled onto the metal side of Au/SiO_2 glass substrates using layer-by-layer liquid phase epitaxy, the details of which have been previously described.[13,52] The Au substrates were treated with an MHDA-SAM layer to improve adhesion. In brief, the substrates were pretreated by O_2 plasma cleaning. The MOF precursors were then iteratively hand-sprayed onto the substrate using a layer-by-layer (LBL) liquid phase epitaxy (LPE) technique. A metallic copper acetate solution (1.0 mM) was sprayed for 15 s followed by a 25 s spray sequence of the polymeric BTC linker (0.2 mM). Residual reactants were washed away with a 5 s rinsing step with pure ethanol after every individual spray sequence. We define a single LBL cycle as both the application of a single round of the metallic and polymeric linker constituents. A total of 125, 150, and 200 cycles resulted in 250, 300, and 400 nm thick films, respectively. Following the completion of all cycle depositions, the MOFs were activated by ultrasonication in dicholormethane and characterized by XRD and IRRAS (see the Supporting Information).

Loading of pristine HKUST-1 thin films with TCNQ and F_4-TCNQ was done following the procedure described by Talin *et al.*[4] The activated pristine MOFs were placed in 2 mM TCNQ (F_4-TCNQ) dissolved in acetonitrile for 72 h. After soaking, they were removed from the loading solution, rinsed with pure acetonitrile (to remove residual loading molecules), and dried with a N_2 flux. XRD data were collected for both sets of guest molecules, showing that the polycrystallinity of the MOF is maintained (see the Supporting

https://doi.org/10.1021/jacs.1c12545
J. Am. Chem. Soc. 2022, 144, 3603−3613

Information). Loading with H_4-TCNQ was not achieved within the thin HKUST-1 because we found that H_4-TCNQ was very volatile and would not stay infiltrated within the pore long enough to acquire measurements.

4.2. Solution Shearing of Bulk HKUST-1. A schematic of the solution shearing method for the deposition of the MOF HKUST-1 films is shown in Figure 7. Coating blade preparation was performed

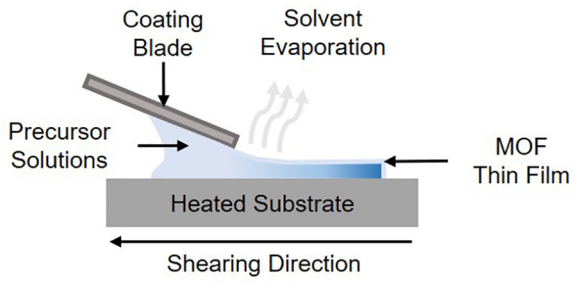

Figure 7. Schematic of the solution shearing method of fabrication and deposition of the thick MOF samples. The MOF self assembles at the leading edge of the shearing blade.

as described in the work of Lee *et al.* and Ghorbanpour *et al.*[31,32] In brief, a silicon wafer was cleaned with toluene, acetone, and isopropyl alcohol. The wafer was exposed to UV-ozone for 10 min. It was immediately treated with 0.1 wt % trichloro(octadecyl)silane in toluene at 50 °C for 24 h. Afterward, the wafer was placed on a hotplate at 85 °C for an hour and was sonicated with acetone for 5 min. The contact angle was measured by using DI water. A well-functionalized coating blade resulted in a contact angle between 95 and 100°.

The precursor solution of HKUST-1 was prepared according to Ameloot *et al.*[53] Copper(II) nitrate hemi(pentahydrate) (1.22 g, 5.25 mmol) was stirred with dimethylsulfoxide (5 mL, 64.0 mmol) until the solution was fully dissolved. Trimesic acid (0.58 g, 2.76 mmol) was added to the solution and mixed until it dissolved completely. The solution produced 0.288 M Cu^{2+} and 0.076 M BTC.

The solution-shearing device used at UVA to fabricate the MOFs was assembled as described in the work of Ghorbanpour *et al.*[32] Before the precursor solution was sheared, the trichloro(octyl)silane (OTS)-functionalized coating blade was washed with toluene, acetone, and isopropyl alcohol and dried with in-house air. The substrate stage was heated to the desired temperature. The blade was held in place with a top vacuum stage, and an 80 nm Au/SiO_2 substrate was attached to the bottom vacuum stage. The blade angle and the gap between the blade and the substrate stage were approximately set to 1° and 100 μm, respectively, by controlling the micro-manipulating assembly. The precursor solution (5−10 μL) of HKUST-1 was injected into the smallest gap between the edge of the blade and the substrate in accordance with the dimensions of the substrate and solution concentration. The solution was deposited on the gold side of the substrate as the blade moved along the substrate. After the blade passed the substrate, samples were taken off from the bottom stage for further analysis by XRD and SEM (see the Supporting Information). The resulting MOFs were approximately 5.5 μm thick.

After HKUST-1 was fully grown on the substrate, it was moved to the N_2-filled glovebox. The HKUST-1 was transferred to the vacuum oven and heated at 180 °C for 12 h. After the heat treatment, the HKUST-1 was cooled down for an hour inside the glovebox. The cooled HKUST-1 was transferred to the saturated TCNQ/F_4-TCNQ/H_4-TCNQ solution (individually) for 72 h.

4.3. Thermal Measurements with Time Domain Thermoreflectance (TDTR). The thermal properties of these samples were measured by time domain thermoreflectance (TDTR), which is described in detail elsewhere.[36,37] For the TDTR measurements, 80 ± 3 nm gold was deposited on top of the SiO_2 substrates by electron beam evaporation at a pressure of 1×10^{-6} Torr and a deposition rate of 1.0 Å/s. The 80 nm Au served to transduce the optical energy from the TDTR laser pulses into thermal energy. TDTR is a time transient, non-contact, optical thermometry technique that utilizes a pump-probe experimental configuration centered around the output of a sub-picosecond (ps) laser system. We used a Ti:sapphire femtosecond Spectra Physics Tsunami oscillator that emits 90 fs pulses at a repetition rate of 80 MHz with a wavelength centered at ∼800 nm (FWHM of 10.5 nm). The pump path was electo-optically modulated with a square wave at a frequency of 8.8 MHz, creating a modulated heating event at the sample surface. The reflectivity of the gold changes linearly with the surface temperature, and this change in reflection was monitored temporally by the time-delayed probe beam. The probe beam was mechanically delayed in time by a translational mechanical delay stage up to 5.5 ns. The reflected intensity from the probe was measured by a photodetector. A lock-in amplifier demodulates the signal and provides amplitude and phase data as a function of pump-probe delay time in the form of a thermal decay curve. These decay curves were fit with a heat conduction model to obtain the thermal properties of the sample.[37,54,55] The pump and probe $1/e^2$ diameters used in our measurements were 22 and 9.5 μm, respectively.

We experimentally measured the heat capacity for the 250 nm pristine HKUST-1 and applied that value to all thicknesses of the pristine HKUST-1, assuming no size dependence in the heat capacity. Furthermore, to support our experimental results, the heat capacity for the infiltrated MOFs was calculated using LD (see the Supporting Information for a full description of the heat capacity measurements and calculations), which agrees well with our experimentally measured pristine value (Figure S6). According to LD, infiltration of a guest molecule increases the volumetric heat capacity upon loading by ∼48%; experimentally, we see that infiltration reduces the thermal conductivity of the pristine MOF by ∼70% (see the Supporting Information for more details about the TDTR experiment).

■ ASSOCIATED CONTENT

Supporting Information

The Supporting Information is available free of charge at https://pubs.acs.org/doi/10.1021/jacs.1c12545.

Contents of the material supplied including characterization data (XRD, SEM, electrical conductivity, TDTR, Raman, FTIR, IRRAS, NMR, pump-probe Brillouin scattering, and nanoindentation) and computational model results (molecular dynamics, lattice dynamics, and spectral energy density) (PDF)

■ AUTHOR INFORMATION

Corresponding Author

Patrick E. Hopkins − *Department of Mechanical and Aerospace Engineering, Department of Material Science and Engineering, Department of Physics, University of Virginia, Charlottesville, Virginia 22904-4746, United States;* orcid.org/0000-0002-3403-743X; Email: phopkins@virginia.edu

Authors

Mallory E. DeCoster − *Department of Mechanical and Aerospace Engineering, University of Virginia, Charlottesville, Virginia 22904-4746, United States;* Present Address: Johns Hopkins University Applied Physics Lab, 11100 Johns Hopkins Rd., Laurel, Maryland 20723, United States; orcid.org/0000-0002-1139-9235

Hasan Babaei − *Department of Chemistry and Chemical and Biomolecular Engineering, University of California, Berkeley, Berkeley, California 94720-1462, United States;* orcid.org/0000-0002-3291-0290

Sangeun S. Jung − *Department of Chemical Engineering, University of Virginia, Charlottesville, Virginia 22904-4746, United States;* orcid.org/0000-0002-0944-7568
Zeinab M. Hassan − *Institute of Functional Interfaces (IF), Karlsruhe Institute of Technology, Karlsruhe 76131, Germany;* Present Address: Chemistry Department, Faculty of Science, Fayoum University, P.O. Box 63514, 63514 Fayoum, Egypt
John T. Gaskins − *Department of Mechanical and Aerospace Engineering, University of Virginia, Charlottesville, Virginia 22904-4746, United States;* Present Address: Laser Thermal Analysis, Inc. 937 2nd St. SE, Charlottesville, Virginia 22902, United States; orcid.org/0000-0001-8622-5902
Ashutosh Giri − *Department of Mechanical and Aerospace Engineering, University of Virginia, Charlottesville, Virginia 22904-4746, United States;* Present Address: College of Engineering, The University of Rhode Island, Kingston, Rhode Island 02881, United States; orcid.org/0000-0002-8899-4964
Emma M. Tiernan − *Department of Mechanical and Aerospace Engineering, University of Virginia, Charlottesville, Virginia 22904-4746, United States*
John A. Tomko − *Department of Mechanical and Aerospace Engineering, University of Virginia, Charlottesville, Virginia 22904-4746, United States;* orcid.org/0000-0001-9260-6568
Helmut Baumgart − *Department of Electrical and Computer Engineering, Old Dominion University, Norfolk, Virginia 23529, United States*
Pamela M. Norris − *Department of Mechanical and Aerospace Engineering, University of Virginia, Charlottesville, Virginia 22904-4746, United States;* Present Address: School of Engineering and Applied Science, George Washington University, Washington, D.C. 20052, United States
Alan J. H. McGaughey − *Department of Mechanical Engineering, Department of Materials Science and Engineering, Carnegie Mellon University, Pittsburgh, Pennsylvania 15213, United States;* orcid.org/0000-0002-0118-6893
Christopher E. Wilmer − *Department of Chemical and Petroleum Engineering, Department of Electrical and Computer Engineering, Clinical and Translational Science Institute, University of Pittsburgh, Pittsburgh, Pennsylvania 15261, United States;* orcid.org/0000-0002-7440-5727
Engelbert Redel − *Institute of Functional Interfaces (IF), Karlsruhe Institute of Technology, Karlsruhe 76131, Germany*
Gaurav Giri − *Department of Chemical Engineering, University of Virginia, Charlottesville, Virginia 22904-4746, United States;* orcid.org/0000-0002-8504-1033

Complete contact information is available at: https://pubs.acs.org/10.1021/jacs.1c12545

Author Contributions

The manuscript was written through contributions of all authors. All authors have given approval to the final version of the manuscript.

Funding

We appreciate funding from the Office of Naval Research, grant no. N00014-20-1-2686. H.B. and C.E.W. gratefully acknowledge support from the National Science Foundation (NSF) awards CBET-1804011 and OAC-1931436. Financial support by Deutsche Forschungsgemeinschaft (DFG) within the COORNETs Priority Program (SPP 1928) is gratefully acknowledged by E.R. and H.B., Z.H. acknowledges financial support from the Egyptian Mission Foundation. A.G. acknowledges funding from the National Science Foundation (NSF Award No. 2119365). A.J.H.M. acknowledges funding from the National Science Foundation (NSF Award No. 2025013).

Notes

The authors declare no competing financial interest.

■ ABBREVIATIONS

MOF metal−organic framework
TDTR time domain thermoreflectance

■ REFERENCES

(1) Xie, L. S.; Skorupskii, G.; Dincă, M. Electrically Conductive Metal−Organic Frameworks. *Chem. Rev.* **2020**, *120*, 8536. acs.chemrev.9b00766 (accessed 2020-09-12) April 10,
(2) Erickson, K. J.; et al. Thin Film Thermoelectric Metal−Organic Framework with High Seebeck Coefficient and Low Thermal Conductivity. *Adv. Mater.* **2015**, *27*, 3453−3459.
(3) Allendorf, M. D.; et al. Guest-Induced Emergent Properties in Metal−Organic Frameworks. *J. Phys. Chem. Lett.* **2015**, *6*, 1182−1195.
(4) Talin, A. A.; et al. Tunable Electrical Conductivity in Metal-Organic Framework Thin-Film Devices. *Science* **2014**, *343*, 66−69.
(5) Redel, E.; Baumgart, H. Thermoelectric porous MOF based hybrid materials. *APL Mater.* **2020**, *8*, No. 060902.
(6) Lee, J.; et al. Metal−organic framework materials as catalysts. *Chem. Soc. Rev.* **2009**, *38*, 1450−1459.
(7) Liu, J.; et al. CO2/H2O Adsorption Equilibrium and Rates on Metal−Organic Frameworks: HKUST-1 and Ni/DOBDC. *Langmuir* **2010**, *26*, 14301−14307.
(8) Abrahams, B. F.; Hoskins, B. F.; Michail, D. M.; Robson, R. Assembly of porphyrin building blocks into network structures with large channels. *Nature* **1994**, *369*, 727−729.
(9) Babaei, H.; McGaughey, A. J. H.; Wilmer, C. E. Effect of pore size and shape on the thermal conductivity of metal-organic frameworks. *Chem. Sci.* **2017**, *8*, 583−589.
(10) Babaei, H.; Wilmer, C. E. Mechanisms of Heat Transfer in Porous Crystals Containing Adsorbed Gases: Applications to Metal-Organic Frameworks. *Phys. Rev. Lett.* **2016**, *116*, No. 025902.
(11) Huang, B. L.; McGaughey, A. J. H.; Kaviany, M. Thermal conductivity of metal-organic framework 5 (MOF-5): Part I. Molecular dynamics simulations. *Int. J. Heat Mass Transfer* **2007**, *50*, 393−404.
(12) Zhang, K.; et al. Alcohol and water adsorption in zeolitic imidazolate frameworks. *Chem. Commun.* **2013**, *49*, 3245−3247.
(13) Babaei, H.; et al. Observation of reduced thermal conductivity in a metal-organic framework due to the presence of adsorbates. *Nat. Commun.* **2020**, *11*, 4010.
(14) Huang, B. L.; Ni, Z.; Millward, A.; McGaughey, A. J. H.; Uher, C.; Kaviany, M.; Yaghi, O. Thermal conductivity of a metal-organic framework (MOF-5): Part II. Measurement. *Int. J. Heat Mass Transfer* **2007**, *50*, 405−411.
(15) Neumann, T.; et al. Superexchange Charge Transport in Loaded Metal Organic Frameworks. *ACS Nano* **2016**, *10*, 7085−7093.
(16) Hopkins, P. E.; Kaehr, B.; Piekos, E. S.; Dunphy, D.; Brinker, C. J. Minimum thermal conductivity considerations in aerogel thin films. *J. Appl. Phys.* **2012**, *111*, 113532−113532.
(17) Sun, L.; et al. A Microporous and Naturally Nanostructured Thermoelectric Metal-Organic Framework with Ultralow Thermal Conductivity. *Joule* **2017**, *1*, 168−177.
(18) Seyf, H. R.; et al. Rethinking phonons: The issue of disorder. *npj Comput. Mater.* **2017**, *3*, 49.

(19) Cheaito, R.; et al. Experimental Investigation of Size Effects on the Thermal Conductivity of Silicon-Germanium Alloy Thin Films. *Phys. Rev. Lett.* **2012**, *109*, 195901−195901.
(20) Toberer, E. S.; Zevalkink, A.; Snyder, G. J. Phonon engineering through crystal chemistry. *J. Mater. Chem.* **2011**, *21*, 15843−15852.
(21) Voneshen, D. J.; Refson, K.; Borissenko, E.; Krisch, M.; Bosak, A.; Piovano, A.; Cemal, E.; Enderle, M.; Gutmann, M. J.; Hoesch, M.; Roger, M. Suppression of thermal conductivity by rattling modes in thermoelectric sodium cobaltate. *Nature Mater* **2013**, *12*, 1028−1032.
(22) Zhuang, J.-L.; Ceglarek, D.; Pethuraj, S.; Terfort, A. Rapid Room-Temperature Synthesis of Metal−Organic Framework HKUST-1 Crystals in Bulk and as Oriented and Patterned Thin Films. *Adv. Funct. Mater.* **2011**, *21*, 1442−1447.
(23) Chen, Y.; Mu, X.; Lester, E.; Wu, T. High efficiency synthesis of HKUST-1 under mild conditions with high BET surface area and CO2 uptake capacity. *Prog. Nat. Sci. Mater. Int.* **2018**, *28*, 584−589.
(24) Prestipino, C.; et al. Local Structure of Framework Cu(II) in HKUST-1 Metallorganic Framework: Spectroscopic Characterization upon Activation and Interaction with Adsorbates. *Chem. Mater.* **2006**, *18*, 1337−1346.
(25) Chui, S. S.-Y.; Lo, S. M.-F.; Charmant, J. P. H.; Orpen, A. G.; Williams, I. D. A Chemically Functionalizable Nanoporous Material [Cu3(TMA)2(H2O)3]n. *Science* **1999**, *283*, 1148−1150.
(26) Gutiérrez-Sevillano, J. J.; Vicent-Luna, J. M.; Dubbeldam, D.; Calero, S. Molecular Mechanisms for Adsorption in Cu-BTC Metal Organic Framework. *J. Phys. Chem. C* **2013**, *117*, 11357−11366.
(27) Bordiga, S.; et al. Adsorption properties of HKUST-1 toward hydrogen and other small molecules monitored by IR. *Phys. Chem. Chem. Phys.* **2007**, *9*, 2676−2685.
(28) Lv, W.; Henry, A. Examining the Validity of the Phonon Gas Model in Amorphous Materials. *Sci. Rep.* **2016**, *6*, 37675.
(29) Allen, P. B.; Feldman, J. L.; Fabian, J.; Wooten, F. Diffusons, locons and propagons: character of atomie yibrations in amorphous Si. *Philos. Mag. B* **1999**, *79*, 1715−1731.
(30) Hendon, C. H.; Walsh, A. Chemical principles underpinning the performance of the metal−organic framework HKUST-1. *Chem. Sci.* **2015**, *6*, 3674−3683.
(31) Lee, J.-C.; Kim, J.-O.; Lee, H.-J.; Shin, B.; Park, S. Meniscus-Guided Control of Supersaturation for the Crystallization of High Quality Metal Organic Framework Thin Films. *Chem. Mater.* **2019**, *31*, 7377−7385.
(32) Ghorbanpour, A.; Huelsenbeck, L. D.; Smilgies, D.-M.; Giri, G. Oriented UiO-66 thin films through solution shearing. *CrystEngComm* **2018**, *20*, 294−300.
(33) Jung, S.; Huelsenbeck, L.; Hu, Q.; Robinson, S.; Giri, G. Conductive, Large-Area, and Continuous 7,7,8,8-Tetracyanoquinodimethane@HKUST-1 Thin Films Fabricated Using Solution Shearing. *ACS Appl. Mater. Interfaces* **2021**, *13*, 10202−10209.
(34) Janiak, C. Demonstration of permanent porosity in flexible and guest-responsive organic zeolite analogs (now called MOFs). *Chem. Commun.* **2013**, *49*, 6933−6937.
(35) Tian, T.; et al. A sol−gel monolithic metal−organic framework with enhanced methane uptake. *Nat. Mater.* **2018**, *17*, 174−179.
(36) Schmidt, A. J. Pump-probe thermoreflectance. *Annu. Rev. Heat Transfer* **2013**, *16*, 159−181.
(37) Cahill, D. G. Analysis of heat flow in layered structures for time-domain thermoreflectance. *Rev. Sci. Instrum.* **2004**, *75*, 5119−5122.
(38) Oberhofer, H.; Blumberger, J. Electronic coupling matrix elements from charge constrained density functional theory calculations using a plane wave basis set. *J. Chem. Phys.* **2010**, *133*, 244105.
(39) Troisi, A.; Nitzan, A.; Ratner, M. A. A rate constant expression for charge transfer through fluctuating bridges. *J. Chem. Phys.* **2003**, *119*, 5782−5788.
(40) Usov, P. M.; et al. Guest−Host Complexes of TCNQ and TCNE with Cu3(1,3,5-benzenetricarboxylate)2. *J. Phys. Chem. C* **2017**, *121*, 26330−26339.
(41) Christensen, M.; et al. Avoided crossing of rattler modes in thermoelectric materials. *Nat. Mater.* **2008**, *7*, 811−815.
(42) Chen, G. *Nanoscale Energy Transport and Conversion: A Parallel Treatment of Electrons, Molecules, Phonons, and Photons*; Oxford University Press: 2005.
(43) Bundschuh, S.; et al. Mechanical properties of metal-organic frameworks: An indentation study on epitaxial thin films. *Appl. Phys. Lett.* **2012**, *101*, 101910.
(44) Van Assche, T. R. C.; et al. High Adsorption Capacities and Two-Step Adsorption of Polar Adsorbates on Copper−Benzene-1,3,5-tricarboxylate Metal−Organic Framework. *J. Phys. Chem. C* **2013**, *117*, 18100−18111.
(45) Li, W.; Carrete, J.; Madsen, G. K. H.; Mingo, N. Influence of the optical-acoustic phonon hybridization on phonon scattering and thermal conductivity. *Phys. Rev. B* **2016**, *93*, 205203.
(46) Li, W.; Mingo, N. Ultralow lattice thermal conductivity of the fully filled skutterudite $YbFe_4Sb_{12}$ due to the flat avoided-crossing filler modes. *Phys. Rev. B* **2015**, *91*, 144304.
(47) Larkin, J. M.; McGaughey, A. J. H. Predicting alloy vibrational mode properties using lattice dynamics calculations, molecular dynamics simulations, and the virtual crystal approximation. *J. Appl. Phys.* **2013**, *114*, 023507−023507.
(48) Allen, P. B.; Feldman, J. L. Thermal conductivity of disordered harmonic solids. *Phys. Rev. B* **1993**, *48*, 12581−12588.
(49) Lv, W.; Henry, A. Direct calculation of modal contributions to thermal conductivity via Green−Kubo modal analysis. *New J. Phys.* **2016**, *18*, No. 013028.
(50) Lundgren, N. W.; Barbalinardo, G.; Donadio, D. Mode Localization and Suppressed Heat Transport in Amorphous Alloys. *Phys. Rev. B: Condens. Matter Mater. Phys.* **2020**, *103*, No. 024204. (December 21, 2020)
(51) Keppens, V.; et al. Localized vibrational modes in metallic solids. *Nature* **1998**, *395*, 876−878.
(52) Arslan, H. K.; et al. High-throughput fabrication of uniform and homogenous MOF coatings. *Adv. Funct. Mater.* **2011**, *21*, 4228−4231.
(53) Ameloot, R.; et al. Direct Patterning of Oriented Metal-Organic Framework Crystals via Control over Crystallization Kinetics in Clear Precursor Solutions. *Adv. Mater.* **2010**, *22*, 2685−2688.
(54) Hopkins, P. E.; et al. Criteria for cross-plane dominated thermal transport in multilayer thin film systems during modulated laser heating. *J. Heat Transfer* **2010**, *132*, 081302−081302.
(55) Schmidt, A. J.; Chen, X.; Chen, G. Pulse accumulation, radial heat conduction, and anisotropic thermal conductivity in pump-probe transient thermoreflectance. *Rev. Sci. Instrum.* **2008**, *79*, 114902−114902.

https://doi.org/10.1021/jacs.1c12545
J. Am. Chem. Soc. 2022, 144, 3603−3613